Parametric assessment of stress development and cracking in internally-cured restrained mortars experiencing autogenous deformations and thermal loading

Kambiz Raoufi[a,*], John Schlitter[b], Dale Bentz[c], and Jason Weiss[d]

[a] PhD Candidate, School of Civil Engineering, Purdue University, 550 Stadium Mall Drive, West Lafayette, IN 47907, USA

[b] MSCE Student, School of Civil Engineering, Purdue University, 550 Stadium Mall Drive, West Lafayette, IN 47907, USA

[c] Chemical Engineer, Engineering Laboratory, National Institute of Standards and Technology, 100 Bureau Dr., Stop 7313, Gaithersburg, MD 20899. E-mail: dale.bentz@nist.gov

[d] Professor, School of Civil Engineering, Purdue University, 550 Stadium Mall Drive, West Lafayette, IN 47907, USA

ABSTRACT

This study used a finite element model to examine how the properties of cementitious mortar are related to the rate of stress development in the dual ring test. The results of this investigation are used to explain the thermal cracking behavior of mixtures containing pre-wetted lightweight aggregates (LWA). In addition to the beneficial effects of using the LWA as an internal curing agent to reduce the autogenous shrinkage of concrete, the LWA also helps to reduce the potential for thermal cracking due to a lower elastic modulus and increased stress relaxation. It was shown that the rate of stress development, age of cracking, and the magnitude of the temperature drop necessary to induce cracking in a dual ring specimen are dependent on a variety of factors, including the coefficient of thermal expansion of both the cementitious mortar and the restraining rings, the elastic modulus of the mortar, the creep effect of the mortar, and the rate of thermal loading. It was shown that depending on the rate of cooling, cracking may or may not occur. The slowest rate of cooling (2.5 °C/h) recommended minimizes the effects of creep while cooling rates faster than 8 °C/h can produce a thermal gradient through the concrete cross section that needs to be considered.

Keywords:

Dual ring, finite element method, thermal cracking, internal curing, lightweight aggregate, and restrained cracking.

* Corresponding author tel.: (765) 494 - 0358; fax: (765) 494 - 0395.
  E-mail address: kambizraoufi@yahoo.com (K. Raoufi).

1. Introduction

When volume changes caused by the heating or cooling of concrete are restrained, residual tensile stresses can develop [1, 2]. These residual stresses can result in cracking if they reach the tensile strength of the concrete. The potential for cracking depends on a combination of a variety of factors including the degree of restraint in the concrete [3], the early-age mechanical property development of concrete [4], the shrinkage of concrete [5], the thermal properties of the concrete (e.g., coefficient of thermal expansion and heat capacity) [6], the heat of hydration [6], the rate of temperature change in concrete [7], and the environmental conditions such as ambient temperature and wind speed [8].

The dual ring test has previously been used to study the stress development and cracking behavior of concrete materials that show shrinkage or expansion at early ages [9-11]. The dual ring test consists of a mortar or concrete specimen that is cast between two concentric restraining rings. If materials for restraining rings are not selected properly in the dual ring test, temperature changes can substantially move the restraint boundaries and alter the degree of restraint. As such, the restraining rings in tests considered in this paper are constructed from Invar 36, a metal alloy with a minimal coefficient of thermal expansion [12-14]. When concrete expands, its expansion is restrained by both the inner and outer Invar rings and a compressive stress is developed in the concrete specimen in the circumferential direction. When the concrete shrinks, it is restrained by the inner Invar ring and tensile stresses develop in the concrete in the circumferential direction. The cracking potential of concrete increases significantly once the residual tensile stress approaches the tensile strength of concrete [5, 15].

Previously, researchers have used the dual-ring test to study the early-age cracking behavior of a cement paste containing a shrinkage-reducing admixture and a cement paste containing an expansive admixture [11, 16, 17]. Bentz et al. [10] used the dual ring to illustrate the influence of cement fineness on restrained shrinkage cracking of hydrating cement paste. Kim et al. [18] have extended the use of a dual ring geometry to study the low-temperature cracking performance of asphalt concrete mixtures. Schlitter et al. [9] used a temperature drop approach to study the thermal cracking of concrete and showed that using pre-wetted LWA is beneficial in improving the thermal cracking resistance of concrete. In this approach, the dual ring geometry was maintained at a constant room temperature for a specific time period; if cracking did not

occur at this point, the temperature was reduced to induce cracking. Schlitter et al. [9] further used the dual ring geometry to characterize early-age expansion behavior and shrinkage cracking performance of concrete containing super absorbent polymers [19].

Restrained thermal and autogenous shrinkage are known as two of the primary contributions to the potential for cracking in concrete members at early ages [2]. Autogenous shrinkage stresses and thermally induced residual stresses can be approximated as being additive [4]. As such, an increase in the magnitude of the shrinkage of concrete makes the concrete more susceptible to thermal induced cracking. Recently, the use of the pre-wetted LWA has been advocated as a method to reduce autogenous shrinkage. The pre-wetted lightweight aggregate serves to increase relative humidity inside the concrete, thereby reducing capillary tension and the associated residual stress development in concrete [20, 21]. Shin et al. [22] have also shown that the use of aggregates with reduced stiffness can improve the shrinkage cracking resistance of concrete due to the combined effects of a lower elastic modulus and higher stress relaxation.

This paper describes the use of finite element simulations to quantify the influence of several material properties on the rate of thermal stress development and cracking potential in the dual ring test. The information from this study will be used to refine how the results of the dual ring test are interpreted, to refine the testing geometry, and to assess how the test should be used in specifications. Further, the impacts of using pre-wetted LWA on improving the thermal cracking performance of concrete are discussed.

2. Modeling approach

Commercial finite element software, FEMMASSE HEAT MLS 8.5*[1], was used to model stress development and cracking in the dual ring test. The finite element model enables stresses, displacements, temperature profile, and cracking to be determined throughout the dual ring geometry. A dual ring geometry, similar to the geometry used by Schlitter et al. [9], was modeled in this study. The geometry consisted of an aging cementitious mortar/concrete ring

---

*[1] Certain commercial equipment, instruments, or materials are identified in this report in order to foster understanding. Such identification is not intended to imply recommendation or endorsement by the National Institute of Standards and Technology nor Purdue University, nor is it intended to imply that the materials or equipment identified are necessarily the best available for the purpose.

that was cast between two concentric Invar rings. The mortar was treated as an aging viscoelastic material, with a cohesive fracture behavior. Age-dependent tensile strength, elastic modulus, σ-w curves (i.e., fracture properties), and autogenous shrinkage were measured separately [23] and used to simulate the mortar/concrete specimen. The approach introduced by Schlitter et al. [9] used cooling at different ages to determine the reserve stress capacity. Time-dependent temperature boundary conditions were used to reduce the temperature of the specimen. Further details on the modeling approach can be found in [24, 25].

The stress development and cracking in the model were compared and calibrated with a similar dual ring experiment [23]. A close agreement was observed between the stress development and cracking in the model and the experiment. The model was then used to perform a sensitivity analysis. The magnitudes of input elastic modulus, the coefficient of thermal expansion, rate of cooling, stress relaxation, autogenous shrinkage, and heat capacity could be varied independently in the model so that the impact of each input property on the stress development and cracking could be determined. The results of the sensitivity analysis were used to explain the influence of pre-wetted lightweight aggregate on the thermal stress development and cracking of concrete specimens.

2.1. A Description of the Modeling Approach

Fig. 1 shows the geometry of the two-dimensional finite element model that was used in this study. The geometry consisted of a mortar/concrete annulus located between two concentric Invar rings. It should be noted that since the geometry of the mortar/concrete specimen is similar to that of the ASTM C1581-09a restrained ring specimen [26], the degree of restraint would be the same [26]. Additional details on how this geometry was developed are given in [9, 27].
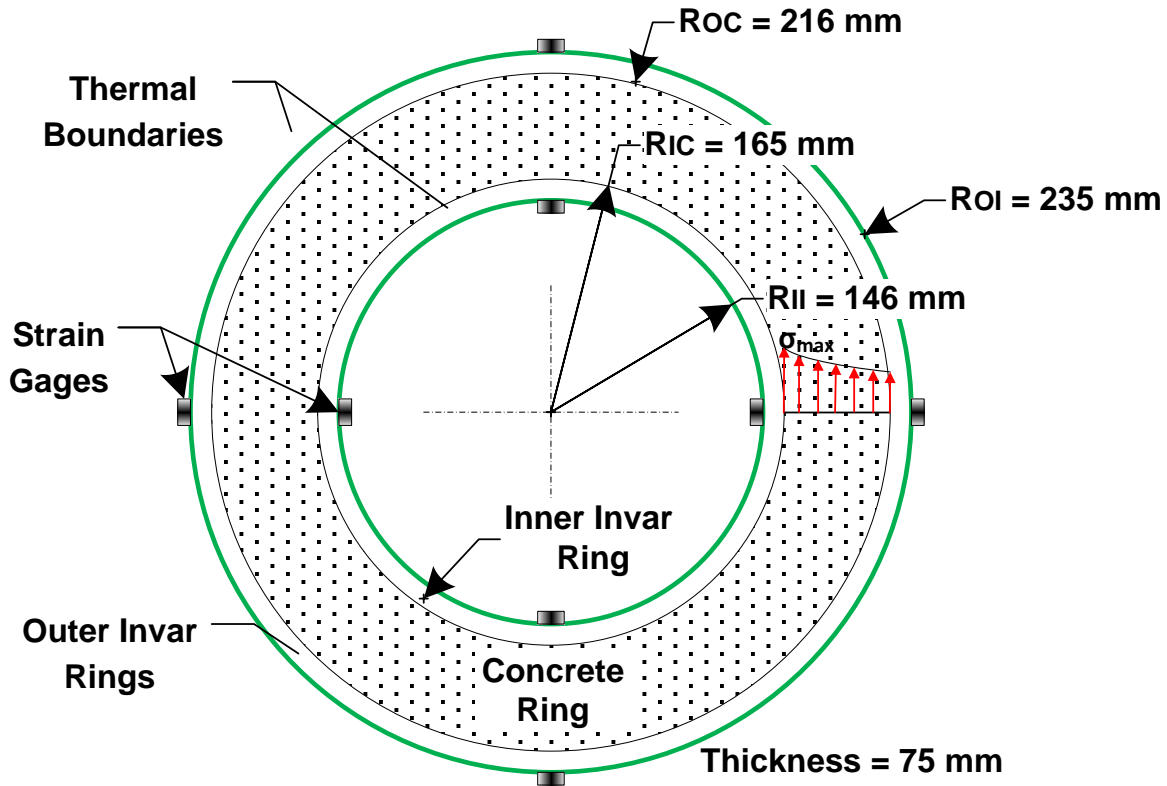
Fig. 1. Schematic overview of the finite element model

Plane stress conditions were assumed. Quadrilateral four-node elements were used in the simulations. The mortar/concrete and Invar rings were all modeled as individual bodies. A series of frictionless cohesionless interface elements were used to model possible separations of the materials at their interface. This is similar to the conditions existing in dual ring experiments [9].

The Invar rings were assumed to remain in their elastic region. Rankine fracture criterion was used to model the formation of a crack in the concrete (i.e., cracking started when the maximum principal stress reached the strength of the concrete). The cohesive zone model was used to describe the post-peak stress-crack opening behavior in the concrete once the crack formed. The crack propagated normal to the direction of maximum principal stress. To control the location of cracking, the strength of a six-degree section of the ring (i.e., like a slice of a pie) was reduced by 10 % and a refined mesh was used in that section.

No moisture exchange was allowed from the concrete to its surrounding environment. The temperatures at the inner surface of the inner Invar ring and the outer surface of the outer Invar ring were prescribed by a defined temperature function. It should be noted that in contrast to conventional convective boundary conditions, the heat transfer coefficient was not considered in this case and the temperature of materials at the boundary was instead defined by the prescribed temperature functions. The temperature of the specimen was maintained at 23 ˚C until the cooling was applied after 48 h from the time of casting at a constant rate of 2.5 ˚C/h (for the baseline case). This procedure is similar to the temperature drop approach that is discussed in [9].

It is worth mentioning that when shrinkage (due to autogenous shrinkage or temperature reduction) of a ring specimen is restrained by an inner ring, tensile stresses develop in the concrete specimen. The maximum tensile stress due to autogenous shrinkage occurs in the circumferential direction at the interface between the specimen and the inner restraining ring (as shown in Fig. 1). Neglecting any creep effect of the concrete and assuming elastic material behavior, the stress development in the specimen is dependent on both the stiffness and the geometry of the concrete and restraining rings, and would decrease as a function of the inverse of the square of the ring radius [28]. Since the concrete is an aging viscoelastic material, the stress relaxation that occurs in the concrete reduces the residual stress development. The magnitude of the stress relaxation depends on the age of concrete, the rate of stress development, the stress level, the duration of loading, the moisture content, and the mechanical properties of concrete.

2.2. Input material properties

The properties used in this study were chosen to represent five mortar mixtures which had a water-to-cement ratio by mass (*w/c*) of 0.30 and 55 % fine aggregate by volume [23]. Two different types of pre-wetted LWA were used in [23] and are designated by LWAK and LWAH in this paper. The mortar mixtures are designated as LWA-0, LWAK-8, LWAK-16, LWAH-12, and LWAH-24 in this paper. LWA-0 represents the plain mortar mixture, while LWAK-8 and LWAK-16 mixtures had 8.25 % and 16.5 % of their total volume replaced with the pre-wetted LWAK aggregates, respectively. Similarly, LWAH-12 and LWAH-24 had 11.85 % and 23.7 %

of their total volume replaced with the pre-wetted LWAH aggregates. It should be mentioned that these LWAK and LWAH aggregates have different water absorption capacities (24 h water absorption of 15.6 % for LWAH and 10.5 % for LWAH). As such, 16.5 % or 23.7 % volumes of LWAK or LWAH in these mortar mixtures provide the same volume of internal curing water and this volume compensates for the chemical shrinkage in these mixtures [20, 23].

Cylindrical specimens (100 mm x 200 mm) were tested to determine the mechanical properties of the mortar mixtures at 1 d, 3 d, and 7 d from the time of casting. It should be noted that all cylindrical specimens were demolded after 24 h and were immediately sealed in plastic bags to prevent water loss. The splitting tensile strength was determined using ASTM C 496-04 [29], while the static elastic modulus was determined according to ASTM C 469-02 [30]. The corrugated tube protocol [31] was used to measure the early age autogenous deformations of the mortar mixtures and ASTM C 403-08 [32] was followed to determine time zero (taken as the time of final set) in this analysis. These material properties were fitted using commercial automated curve fitting software [33], and were used as input values to simulate the mortar behavior at early ages. Fig. 2, 3 and 4 summarize these input material properties. It can be seen in Fig. 2 and 3 that the elastic modulus and tensile strength of the mortar decreased as the volume replacement of the pre-wetted LWA in the mortar increased. Further details on mixture proportions, testing procedures and measuring material properties can be found in [23].

To determine the coefficient of thermal expansion (COTE) for the specimens, two mortar prisms (25 mm × 25 mm × 285 mm) were cast for each mortar mixture. The prisms were prepared according to ASTM C490-09 [34]. All prisms were demolded after 24 h. They were immediately sealed using aluminum tape after demolding to prevent water loss and cured at 23 ℃ for seven days. As specified by ASTM C490-09 [34], a digital dial gage with a precision of 0.001 mm was used to measure the length of specimens. The temperature of the specimens was changed from 23 ℃ to 10 ℃ and the length was measured after 24 h. The temperature was then changed to 38 ℃ and the length of the specimens was determined after another 24 h. The lengths of the specimens at 10 ℃, 23 ℃, and 38 ℃ were used to determine the COTE. Measurements indicated that all mortar mixtures had a similar COTE, and the COTE of these mixtures did not appear to be statistically sensitive to the presence of the LWAs that were used

in this study [35-37]. Based on these experiments, an average COTE value of 14 $\mu\varepsilon/°C$ was used to model thermal deformations of the mortar mixtures in the simulations.

A constant volumetric heat capacity of 2100 $kJ/(m^3 \cdot K)$ [9] and a constant thermal conductivity of 1.8 $W/(m \cdot K)$ [38] were used to characterize the thermo-physical properties of the mortar specimens.

A wedge splitting test was performed according to the procedure outlined in [39] to determine fracture properties of these mixtures. It was determined that these mixtures had a similar shape for their softening curves, and a bilinear softening curve was used to characterize the post-peak behavior of these materials in this investigation. The softening relationship was characterized by a knee point with a stress-to-strength ratio of 0.35 and a crack width of 0.01 mm, and a critical crack width of 0.08 mm.

An age-dependent Maxwell Chain Model with four Maxwell elements was used to model stress relaxation and creep [40]. The fourth unit in the Maxwell Chain Model consisted of a spring to better model the aging viscoelastic behavior of the specimen [25]. To estimate the coefficients of the Maxwell Chain Model, the stress development in the model was compared with the stress development in a dual ring experiment [23]. The coefficients of the Maxwell units were selected to have a similar residual stress development in the dual ring model and the experiment. The coefficients of the Maxwell units can be found in [24].

Invar rings were assumed to have a constant elastic modulus of 141 GPa, a constant Poisson's ratio of 0.30, and a constant COTE of 1.30 $\mu\varepsilon/°C$ [9, 12, 13].
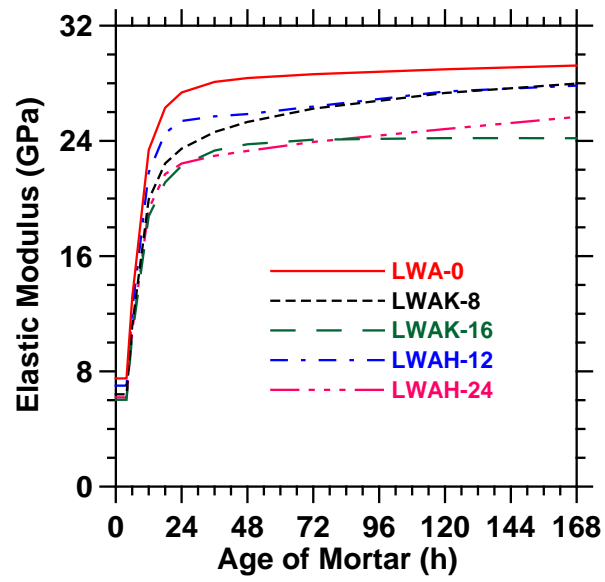
Fig. 2. Elastic modulus development of mortar mixtures (fitted) [23]
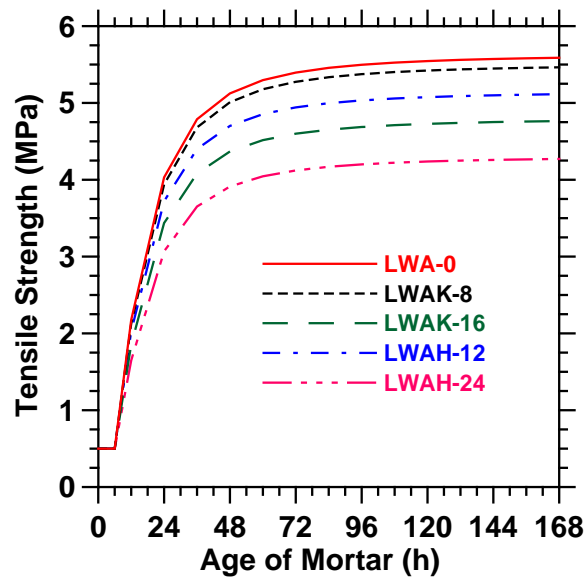
Fig. 3. Tensile strength development of mortar mixtures (fitted) [23]

10
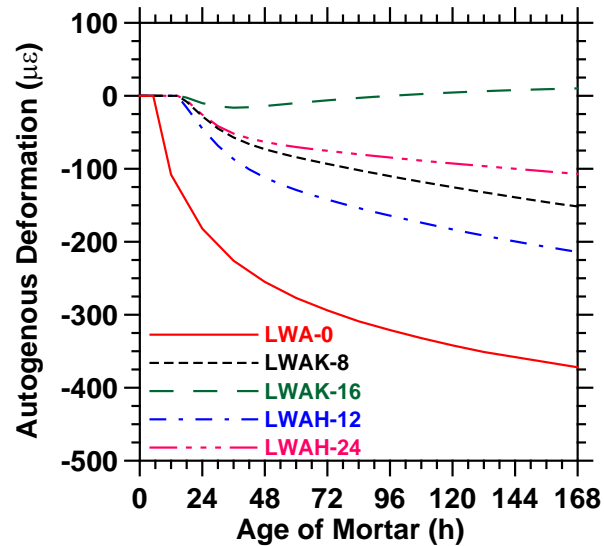
Fig. 4. Fitted autogenous shrinkage development of plain mortar and mortars with the pre-wetted LWAs [23]

3. Thermal cracking in dual ring specimens

Schlitter et al. [9] used the dual ring test to study the cracking behavior of concrete mixtures that experience early-age autogenous shrinkage or expansion while undergoing temperature changes. The rings were initially cured at constant temperature of 23 °C. At a specific age cooling of the specimens was initiated at constant rate of 2.5 °C/h until the specimen cracked or the lower temperature limit of the experimental set up was reached. The magnitude of the temperature drop was used to quantify the thermal cracking resistance of a concrete mixture at that age. A similar procedure was used in this study. This approach is illustrated in Fig. 5. The specimen was initially maintained at a constant temperature of 23 °C for the first 48 h. During this time period, no stress was developed in the specimen other than autogenous shrinkage-induced stress (which was assumed to be zero for the base case model shown in Fig. 5). Cooling of the specimen began at 48 h at the rate of 2.5 °C/h (Fig. 5a). When the cooling began, thermal deformations were restrained by the inner Invar ring, resulting in the development of tensile stresses in the specimen. A small temperature difference of 0.3 °C was observed between the outside circumference and the center of the specimens during the cooling phase. As such, the temperature distribution can be assumed to be uniform through the concrete section. The simulated strength development and average tensile stress (i.e., average stress along the radial

direction) in the concrete specimen are illustrated in Fig. 5b. It should be noted that the average tensile stress values in this study were calculated as the average of circumferential stress values at 10 equi-distance locations along the radial direction of the concrete specimen and outside of the reduced strength zone [5]. Once the cooling started at 48 h, the rate of stress development increased to 0.45 MPa/h. Cracking occurred once the calculated average stress approached the tensile strength and reached a peak stress value. The peak average stress value is referred to as the failure stress in this paper. Cracking of the ring specimen is marked by a sharp drop in the average stress curve as illustrated in Fig. 5b. In the base case simulation, cracking occurred 11 h after the cooling began, at which time the temperature of the specimen was 10.5 ˚C. This corresponded to a temperature drop of 12.5 ˚C (i.e., 23 ˚C – 10.5 ˚C = 12.5 ˚C).
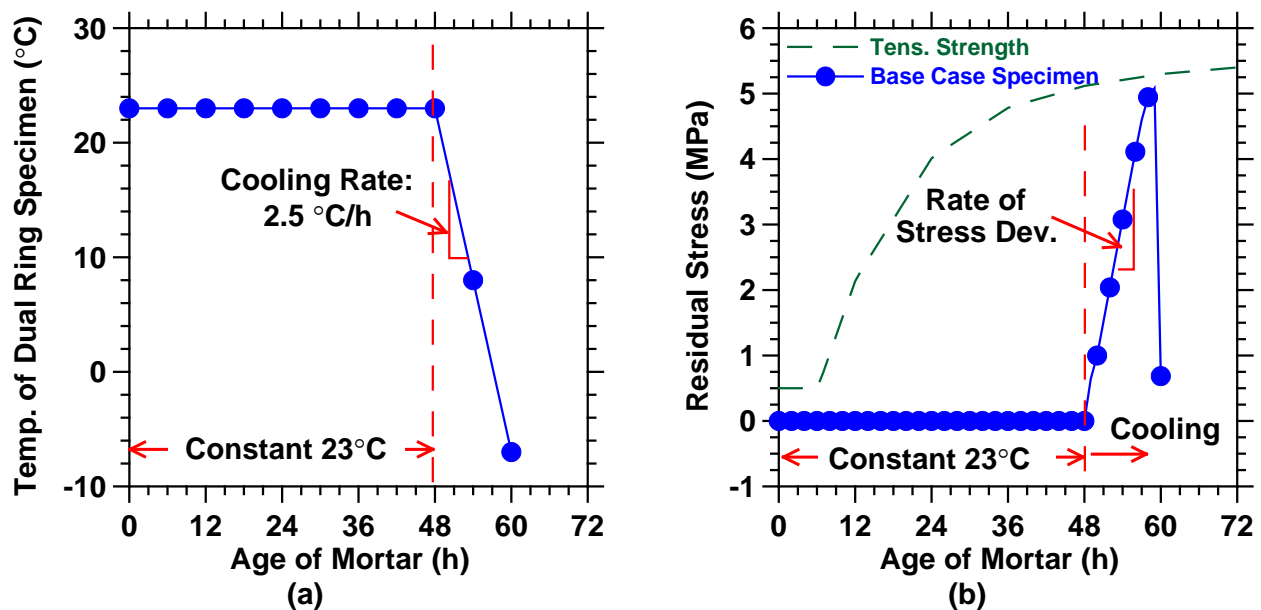
Fig. 5. (a) Temperature profile and (b) average residual stress development in base case specimen when cooled at 48 h.

To better explain the cracking behavior and stress development in the dual ring specimen, the crack opening displacement and stress distribution in the reduced strength region of the reference (base case) ring specimen are shown in Fig. 6. It can be seen that the stress reached the strength of concrete at the inner circumference of the specimen and cracking initiated at 55 h. The length of the crack can be determined by locating the maximum stress value at each time and its

distance from the inner surface of the ring. The crack propagated in a stable fashion between 55 h and 58 h. During this same time period, the length of the crack grew to 45 mm through the concrete section, which is 50 mm thick. The average section stress increased while a small crack opening displacement was observed. At 58 h, the crack propagation phase began. During this phase, the crack opening displacement began to increase at a faster rate and stresses began to decrease through the mortar wall. Once the crack opening displacement exceeded the critical crack width of 0.08 mm, the crack became traction free and the specimen began to deform freely.
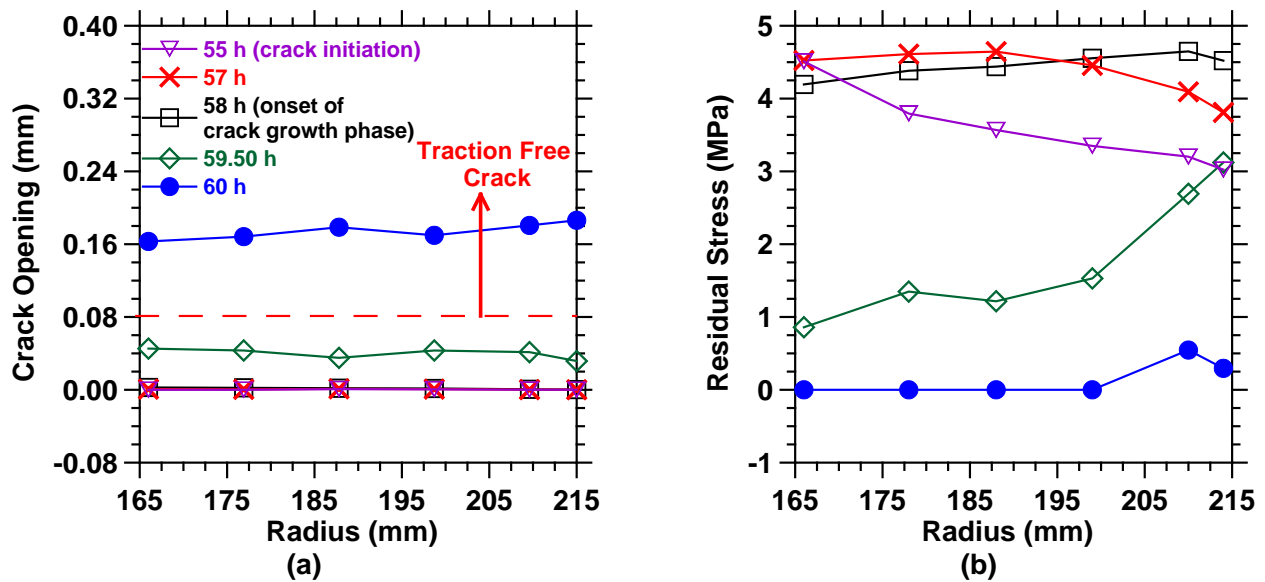
Fig. 6. (a) Crack opening displacement and (b) average residual stress profile in the reduced strength section of the base case ring specimen when cooled at 48 h.

Fig. 7 compares calculated stresses in the plain mortar specimen and the specimens containing different volumes and types of the pre-wetted LWA. Fig. 7 shows that each mortar specimen experienced a different rate and magnitude of stress development after the time of set. The differences in the rate of stress development can be attributed to different age-dependent mortar elastic modulus (Fig. 2a), stress relaxation, and autogenous shrinkage development in these mixtures (Fig. 4). For example, the plain mortar specimen (LWA-0) had the highest elastic modulus and autogenous shrinkage, which lead to the highest rate and magnitude of stress development. On the other hand, the LWAK-16 specimen developed a compressive stress at

early ages due to its early-age autogenous expansion (Fig. 4). The cooling began at 48 h in all cases. After the cooling began, thermal stresses began to be superimposed on the already developing shrinkage stresses and the differences in rate of stress development were further magnified. This behavior is consistent with experimental observations as reported by Schlitter et al. [27]. Consequently, several additional factors such as the coefficient of thermal expansion, rate of heating, heat capacity, and thermal conductivity can further influence the stress development in these materials. This research is aimed at quantifying the individual influences of each of these factors on the stress development and cracking behavior in the dual ring specimen test.
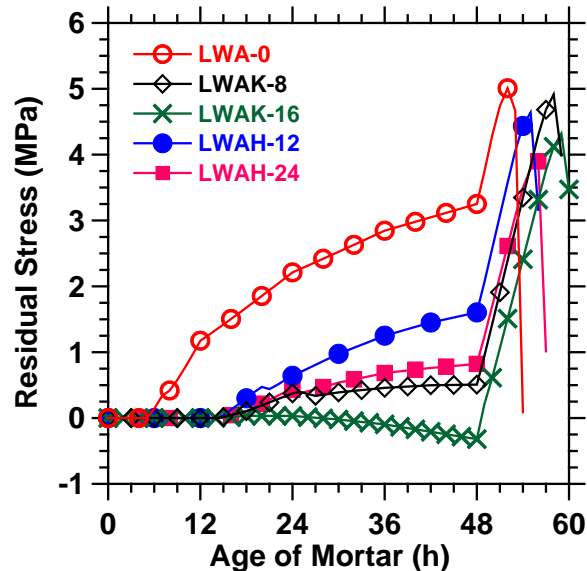
Fig. 7. Calculated residual stress development in dual-ring specimens when cooling began after 48 h.

4. Sensitivity Analysis

In order to determine the sensitivity of the dual ring test to different testing conditions and material properties, seven series of simulations were performed. Only one factor was varied in each series, while all other mixture properties were kept the same as those of the plain mortar mixture. This allowed the influence of each factor on the rate of stress development, failure

stress, the age of cracking, and the thermal resistance of the dual ring specimen to be determined. The simulations and results are summarized in Table 1. As shown in Table 1, the influence of the concrete's elastic modulus, the COTE of mortar mixtures, the COTE of the metal rings, the rate of cooling, the stress relaxation of concrete, the autogenous shrinkage of concrete, and the concrete's volumetric heat capacity on stress development and cracking behavior were investigated in this sensitivity analysis. The grey-shaded areas in Table 1 indicate cases where the rate of stress development and the magnitude of the temperature drop to induce cracking were highly sensitive to changes in a particular variable. These simulations are discussed in the following sections. Since the model does not contain many cross-product terms that are based on the input parameters, no significant effects on the rate of stress development were found when multiple factors were varied at the same time (i.e., two factor interactions were determined to be negligible).

Table 1. Summary of the performed simulations and results.

Simulation ID	Variable	Change in Elastic Mod.	Change in Concrete COTE	Change in Invar COTE	Change in Rate of Cooling	Change in Stress Relax.	Change in Autog. Shrink.	Change in Heat Capacity	Change in Failure Stress	Change in Age of Cracking	Change in Rate of Stress Dev	Change in Temp. Drop
Base Case	–	*0%*	*0%*	*0%*	*0%*	*0%*	*No Shr.*	*0%*	*0.0%*	*0.0%*	*0.0%*	*0.0%*
E-12	Elastic Modulus (Sec. 5.1)	-60%	0%	0%	0%	0%	No Shr.	0%	-13.3%	13.6%	-54.7%	72.7%
E-18		-40%	0%	0%	0%	0%	No Shr.	0%	-6.7%	6.8%	-32.0%	36.4%
E-24		-20%	0%	0%	0%	0%	No Shr.	0%	-2.9%	1.7%	-15.0%	9.1%
E-37		20%	0%	0%	0%	0%	No Shr.	0%	0.4%	-1.7%	13.3%	-9.1%
E-43		40%	0%	0%	0%	0%	No Shr.	0%	0.8%	-3.4%	25.4%	-18.2%
E-49		60%	0%	0%	0%	0%	No Shr.	0%	0.8%	-5.1%	36.1%	-27.3%
COTE-2	COTE of Concrete (Sec. 5.2)	0%	-86%	0%	0%	0%	No Shr.	0%	NA	NA	-92.7%	NA
COTE-4		0%	-71%	0%	0%	0%	No Shr.	0%	-9.7%	55.9%	-70.8%	300.0%
COTE-6		0%	-57%	0%	0%	0%	No Shr.	0%	-6.1%	27.1%	-60.4%	145.5%
COTE-10		0%	-29%	0%	0%	0%	No Shr.	0%	-2.4%	8.5%	-31.5%	45.5%
COTE-18		0%	29%	0%	0%	0%	No Shr.	0%	-0.4%	-3.4%	31.9%	-18.2%
COTE-24		0%	71%	0%	0%	0%	No Shr.	0%	0.3%	-6.8%	84.9%	-36.4%
COTErest-0	COTE of Invar (Sec. 5.2)	0%	0%	-100%	0%	0%	No Shr.	0%	0.2%	0.0%	10.6%	0.0%
COTErest-7		0%	0%	438%	0%	0%	No Shr.	0%	-3.7%	13.6%	-45.8%	72.7%
COTErest-12		0%	0%	823%	0%	0%	No Shr.	0%	-10.5%	81.4%	-81.0%	436.4%
COTErest-18		0%	0%	1285%	0%	0%	No Shr.	0%	NA	NA	-103.2%	NA
Q-0.5	Rate of Cooling (Sec. 5.3)	0%	0%	0%	-80%	0%	No Shr.	0%	-5.9%	64.4%	-72.3%	345.5%
Q-1		0%	0%	0%	-60%	0%	No Shr.	0%	-3.8%	23.7%	-57.2%	127.3%
Q-2		0%	0%	0%	-20%	0%	No Shr.	0%	-1.2%	5.1%	-20.0%	27.3%
Q-3		0%	0%	0%	20%	0%	No Shr.	0%	0.1%	-1.7%	20.2%	-9.1%
Q-4		0%	0%	0%	60%	0%	No Shr.	0%	0.4%	-5.1%	65.3%	-27.3%
Q-5		0%	0%	0%	100%	0%	No Shr.	0%	-0.3%	-6.8%	106.6%	-36.4%
Q-6		0%	0%	0%	220%	0%	No Shr.	0%	-1.4%	-11.9%	225.2%	-63.6%
Q-7		0%	0%	0%	300%	0%	No Shr.	0%	-0.8%	-13.6%	307.8%	-72.7%
R-5	Stress Relaxation (Sec. 5.4)	0%	0%	0%	0%	-5%	No Shr.	0%	-0.9%	1.7%	-5.2%	9.1%
R-13		0%	0%	0%	0%	-13%	No Shr.	0%	-1.6%	3.4%	-10.8%	18.2%
R-22		0%	0%	0%	0%	-22%	No Shr.	0%	-2.5%	5.1%	-16.5%	27.3%
R-32		0%	0%	0%	0%	-32%	No Shr.	0%	-4.6%	8.5%	-22.2%	45.5%
R-42		0%	0%	0%	0%	-42%	No Shr.	0%	-7.0%	16.9%	-28.6%	90.9%
S+102	Autogenous Shrinkage (Sec. 5.5)	0%	0%	0%	0%	0%	-140%	0%	-1.5%	3.4%	5.2%	18.2%
S+51		0%	0%	0%	0%	0%	-120%	0%	-0.4%	1.7%	5.3%	9.1%
S-102		0%	0%	0%	0%	0%	-60%	0%	-0.6%	-5.1%	4.9%	-27.3%
S-153		0%	0%	0%	0%	0%	-40%	0%	-0.5%	-6.8%	5.6%	-36.4%
S-204		0%	0%	0%	0%	0%	-20%	0%	-1.3%	-8.5%	5.3%	-45.5%
Plain-48		0%	0%	0%	0%	0%	0%	0%	-1.5%	-11.9%	1.5%	-63.6%
S-306		0%	0%	0%	0%	0%	20%	0%	-0.9%	-13.6%	-7.3%	-72.7%
S-357		0%	0%	0%	0%	0%	40%	0%	-20.3%	-35.6%	NA	NA
S-408		0%	0%	0%	0%	0%	60%	0%	-39.9%	-64.4%	NA	NA
C-1260	Heat Capacity (Sec. 5.6)	0%	0%	0%	0%	0%	No Shr.	-20%	0.0%	0.0%	0.4%	0.0%
C-1680		0%	0%	0%	0%	0%	No Shr.	-10%	0.0%	0.0%	0.3%	0.0%
C-2520		0%	0%	0%	0%	0%	No Shr.	10%	0.0%	0.0%	-0.2%	0.0%
C-2940		0%	0%	0%	0%	0%	No Shr.	20%	0.0%	0.0%	-0.4%	0.0%

4.1. Influence of elastic modulus

The elastic modulus influences the results in two ways when the pre-wetted lightweight aggregate is added to the mortar. First, the addition of the lower stiffness lightweight aggregate reduces the elastic modulus of the composite [22, 41]. Second, the internal curing water stored inside lightweight aggregates increases the cement hydration and thereby increases the elastic

modulus of the matrix accordingly [42]. The net effect is generally a reduction in elastic modulus as shown in Fig. 2 [23]. To determine the role of elastic modulus on the stress development and cracking in the dual ring specimen, six simulations were performed. The elastic modulus of plain mortar was altered by ±20 %, ±40 %, and ±60 % in these simulations while all other mortar properties were held the same as that of the base case specimen (Table 1).

Fig. 8a shows the influence of elastic modulus on the rate of stress development in the dual ring specimen. In the absence of shrinkage deformation, no residual stress was developed before the cooling began, and stresses were developed starting at 48 h. Fig. 8a shows that with increasing the mortar elastic modulus, the rate of stress development increased and the specimen cracked earlier. When the mortar elastic modulus was reduced to 40 % of its initial magnitude, stresses developed at a rate of 0.25 MPa/h while stresses developed at a rate of 0.69 MPa/h when the elastic modulus was increased to 160 % of its baseline value. It should be noted that three phenomena occurred when altering the elastic modulus of the mortar specimen. First, the degree of restraint of the dual ring test decreased with an increase in the mortar elastic modulus [5, 43]. Reducing the degree of restraint acts to reduce the stress developed for a given strain value. However, the second effect involves a direct increase of stress development in the specimen for a given strain due to Hooke's Law.   The third effect, which was less significant than the other two effects, included an increase in stress relaxation with increasing the elastic modulus. The second effect has a greater influence on stress development, therefore the observed rate of stress development increased with an increase in the elastic modulus of the mortar specimen.

The effect of elastic modulus on the magnitude of the temperature drop to induce cracking and average section stress of the specimen at failure is shown in Fig. 8b. As the elastic modulus was reduced, stresses developed more slowly and a larger temperature drop was needed to crack the specimen. It should be noted that the magnitude of the temperature drop started to increase at a greater rate when the mortar elastic modulus was reduced below 80 % of the plain mortar elastic modulus. This behavior can be attributed to a higher stress relaxation and creep in mortar specimens with lower elastic modulus values. It should be noted that the stress relaxation was increased when the specimen cracked at a later age.
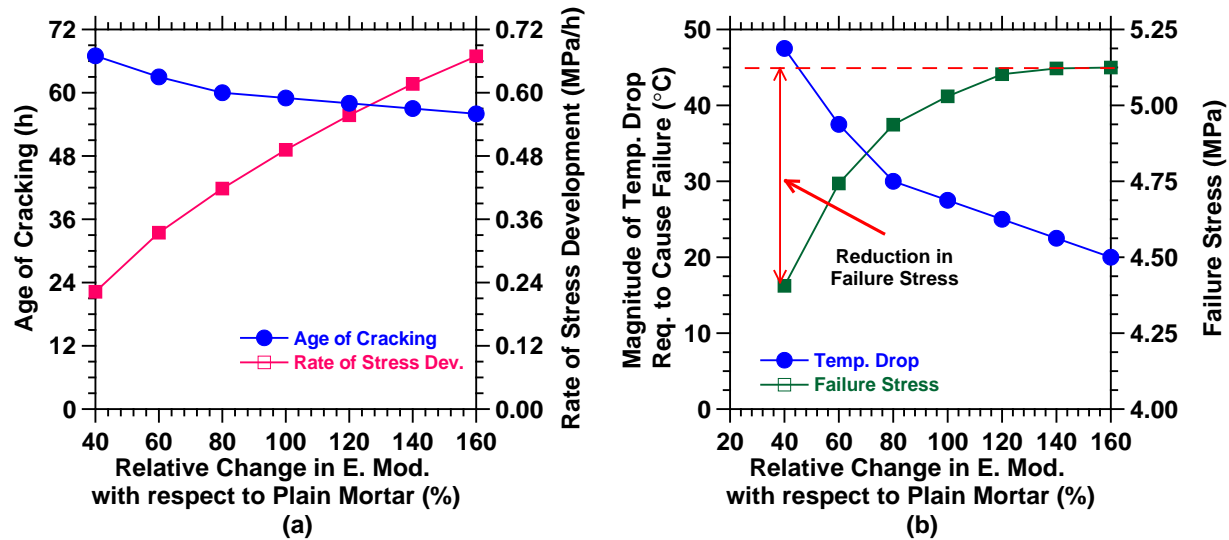
Fig. 8. Influence of elastic modulus of the specimen on (a) the residual stress development, age of cracking, (b) the magnitude of temperature drop, and the reduction in strength.

Fig. 8b shows that the average stress of the specimen at failure was reduced with an increasing elastic modulus. To explain the influence of elastic modulus on the failure stress and stress distribution in the specimen, the stress distribution and crack opening displacement through the wall of the concrete ring are shown in Fig. 9 during the stable and unstable crack propagations. It can be seen in Fig. 9 that considerable crack opening and unloading began to occur in the cracked region as the crack grew in size. The unloading and crack opening were more significant in the specimens with reduced elastic modulus (Fig. 8) than in the base case (Fig. 6). The greater unloading of the cracked specimen can be explained by the existence of a more compliant crack in specimens with a lower elastic modulus. As the elastic modulus of the specimen was reduced, its stiffness was reduced, crack opening displacement increased, and stress transfer and softening through surfaces of a crack were reduced. As such, the failure stress (average section stress at the onset of unstable cracking) was reduced with decreasing elastic modulus. Due to additional effect of stress relaxation, the effect of elastic modulus on reducing the average stress at failure of the specimen became more significant when the reduction in the mortar elastic modulus exceeded 20 %.
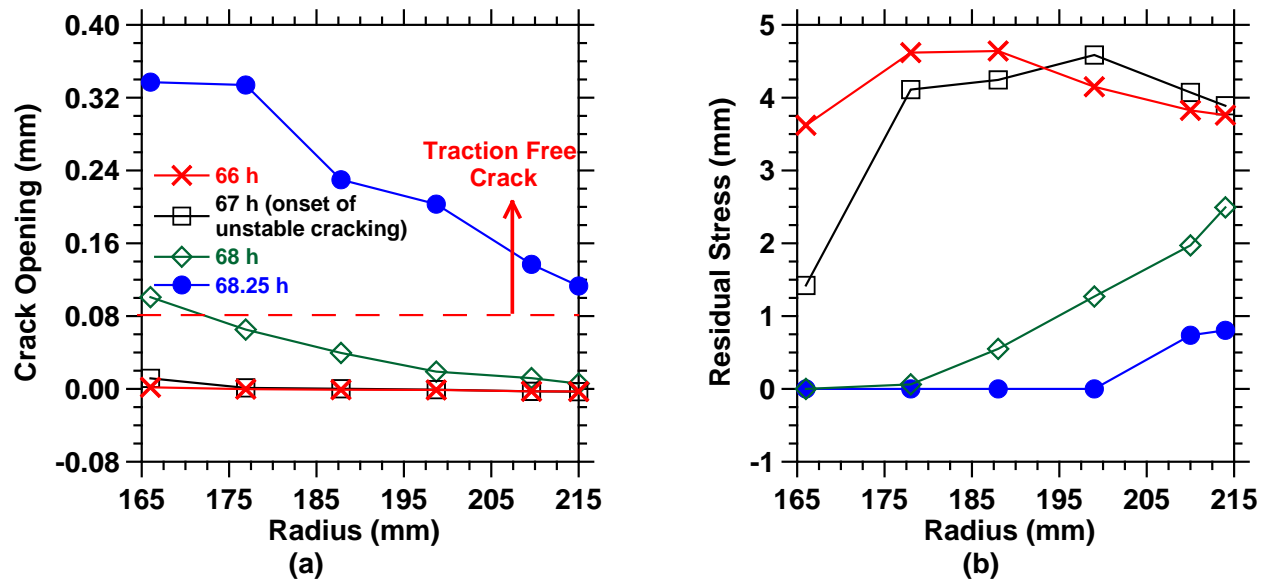
Fig. 9. (a) Crack opening displacement and (b) residual stress development through the specimen wall in the damage zone when the elastic modulus was reduced by 60 %.

4.2. Influence of coefficient of thermal expansion of Invar and concrete

When the dual ring was cooled, both the concrete and the two restraining rings underwent different rates of thermal deformations as based on their respective COTEs. As such, the rate of thermal stress development was greatly dependent on the COTEs of the mortar material and restraining rings. Although a similar linear COTE of 14 µε/°C was used for all mortar mixtures in this study, it must be mentioned that the COTE is highly dependent on the aggregate composition, aggregate volume, moisture content, and the presence of LWA particles [2, 44, 45]. It has been reported that a concrete with lightweight aggregates generally has a smaller COTE than that of a concrete with normal weight aggregates [35-37]. This however was not observed in the mortars examined in this investigation.

To determine the sensitivity of the dual ring test to the COTE of the mortar, a series of simulations was performed. The COTE of the mortar specimen was varied from 2 µε/°C to 24 µε/°C as shown in Table 1. The effect of the COTE on the stress development and cracking behavior is shown in Fig. 10a. As expected, the rate of stress development (i.e., the slope of the residual stress versus time curve) was found to increase with increasing the COTE of the

specimen. While thermal stresses in the specimen with a COTE of 24 µε/˚C increased at a rate of 0.91 MPa/h, the rate of stress development was diminished to 0.04 MPa/h when the COTE was reduced to 2 µε/˚C. Cracking occurred at an earlier age when the COTE of the mortar increased. Cracking occurred after 11 h of cooling in the base case specimen, while no cracking occurred after 48 h of cooling when the COTE of the mortar was reduced to 2 µε/˚C. It is further noticed that the average section stress of the ring specimens at failure was reduced as the COTE of the mortar and the rate of stress development were reduced. This reduction in the average stress of the ring specimens at failure can be attributed to higher stress relaxation and the corresponding stress redistribution along the radial direction in these specimens [46-48].

Restraining rings can theoretically be made from any material. If the COTE of the restraining ring is higher than that of the concrete, the restraining rings shrink more than the specimen upon cooling, and the outer restraining ring would apply a compressive force on the specimen. Five series of simulations were performed in addition to the base case (i.e., the Invar rings) to determine the influence of the COTE of the restraining rings on stress development in the dual ring test. Restraining rings with COTE values of 0 µε/˚C, 1.3 µε/˚C (Invar), 7 µε/˚C, 12 µε/˚C (COTE for a typical steel), and 18 µε/˚C were simulated. Fig. 10b illustrates the effect of the COTE of the restraining ring on the stress development in the dual ring specimen. It can be seen that when the COTE of the restraining rings approached that of the concrete, the rate of stress development in the specimen was greatly reduced. It should be noted that no stress would develop in the specimen if both concrete and restraining rings have the same COTE. As shown by the $COTE_{rest}$ – 18 curve in Fig. 10b, a compressive stress started to develop in the specimen under cooling once the COTE of restraining rings exceeded that of the concrete specimen.
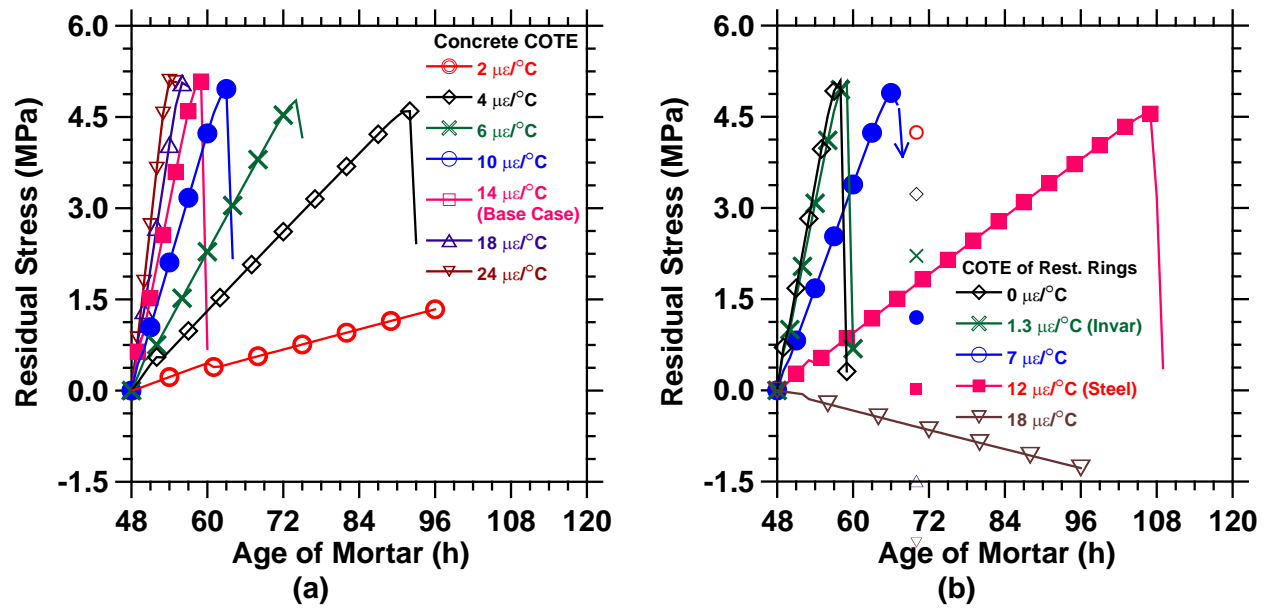
Fig. 10. Influence of (a) COTE of the mortar specimen and (b) COTE of restraining rings on the average residual stress development.

Fig. 11a shows the influence of the relative thermal deformations of the specimen and the restraining ring (as shown by the difference between their COTEs) on the stress development and age of cracking. It can be seen that the rate of stress development was proportional to the difference between the COTEs of the mortar specimen and the restraining rings. As expected, as the difference between the COTEs of the specimen and the restraining rings was reduced, the rate of stress development was reduced, and the specimen became less prone to cracking.

It can be seen that while low-carbon steel materials with a COTE of 12 µε/°C can provide sufficient stiffness and are conveniently used in the conventional restraining ring test (which is done at a constant temperature) such as ASTM 1581-09a [26], it may not be so suitable to study the thermal cracking behavior of concrete in the dual ring test. Since the COTE for concrete typically varies between 5-15 µε/°C [35, 36], using restraining rings with a high COTE such as low-carbon steel may not be appropriate in dual ring test (Fig. 11b). When restraining rings with such a high COTE are used, the restraint moves substantially with temperature variations, a higher extent of stress relaxation occurs, the average section stress of the specimen at failure is reduced, and a higher temperature drop is needed to crack the specimen. Consequently, the

thermal cracking performance of concrete would be better assessed using restraining rings with a lower COTE, such as those made from Invar.
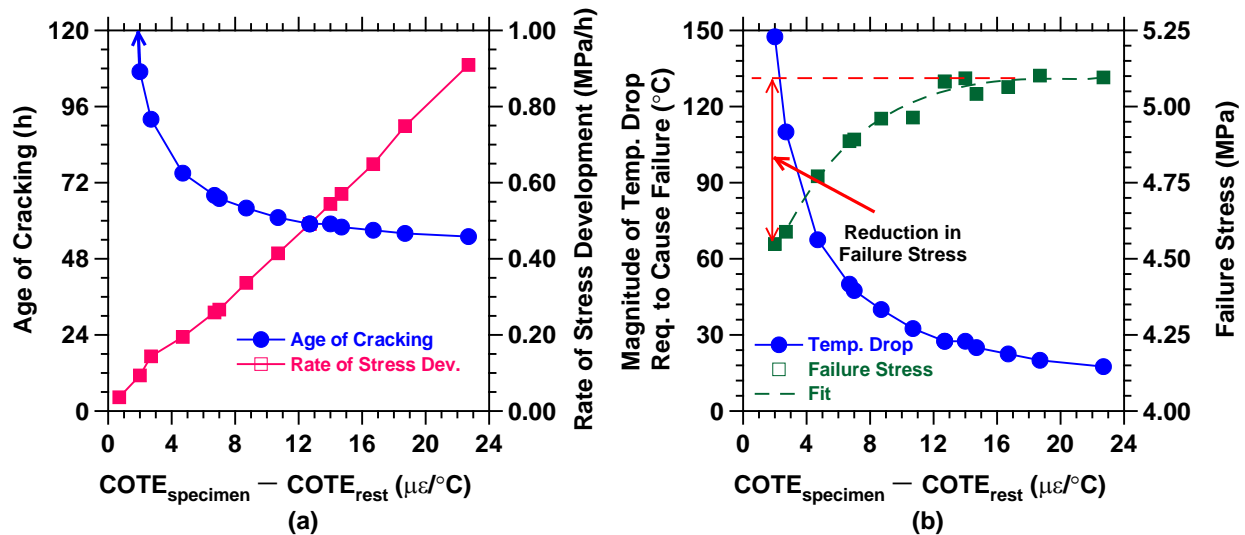
Fig. 11. Influence of relative thermal deformations of the mortar and restraining rings on (a) the rate of stress development, age of cracking, (b) the magnitude of temperature drop, and the reduction in average stress of dual ring specimen at failure.

4.3. Influence of the rate of cooling

The influence of the rate of loading on the failure stress of concrete has been studied by various researchers in the past [46, 47, 49-51]. When the loading rate is reduced, stresses in concrete are relaxed due to effects of creep of concrete under sustained load, stresses are redistributed, and the average stress of specimens at failure is generally reduced [47, 50, 51]. A series of simulations was performed to quantify the influence of the rate of cooling on stress development in the dual ring test. Five cooling rates of (0.5, 1.0, 2.0, 3.0, 5.0, 8.0 and 10.0) °C/h were simulated in this series in addition to the base case cooling rate of 2.5 °C/h, as indicated in Table 1. No shrinkage was considered in the simulations and the cooling started at 48 h.

Fig. 12a illustrates the influence of the rate of cooling on the stress development and cracking in the dual-ring test. As expected, the rate of stress development in the specimen increased with an increase in the rate of cooling. When the temperature was reduced at a faster rate, the thermal

stresses developed faster, and cracking occurred at an earlier age. While a minimal temperature gradient of 0.3 °C was observed in the base case specimen, the temperature difference between the center and outer surfaces of the specimens exceeded 1 °C when the cooling rate exceeded 8.0 °C/h. As such, it is recommended to keep the cooling rate below 8.0 °C/h to limit the thermal stress gradient through the concrete cross section. It should be noted that this rate of cooling is well above the cooling capacity of most conventional cooling devices and the highest rate of cooling will likely be limited by the cooling device.

Fig. 12b shows that the magnitude of the temperature drop necessary to induce cracking was highly dependent on the rate of cooling. As the cooling rate was reduced, a higher magnitude of temperature drop was needed to crack the specimen. The magnitude of the temperature drop increased significantly once the cooling rate became smaller than 2.5 °C/h. For example, while only a temperature drop of 27.5 °C was needed to crack the specimen at the cooling rate of 2.5 °C/h, the computed magnitude of the temperature drop was increased to 122.5 °C at the cooling rate of 0.5 °C/h. As such, a specimen may or may not crack in the dual ring test depending on the cooling rate. The influence of the cooling rate on average stress of the specimen at failure is shown in Fig. 12b. The failure load of the specimen began to decrease once the loading rate became smaller than 2.5 °C/h and specimens began to crack at noticeably later ages. The stress relaxation of concrete increased as specimens cracked at later ages. The higher stress relaxation resulted in the formation of more compliant cracks and the corresponding stress redistribution. The stress redistribution reduced the average stress through the cross section at failure, as the rate of thermal loading decreased.
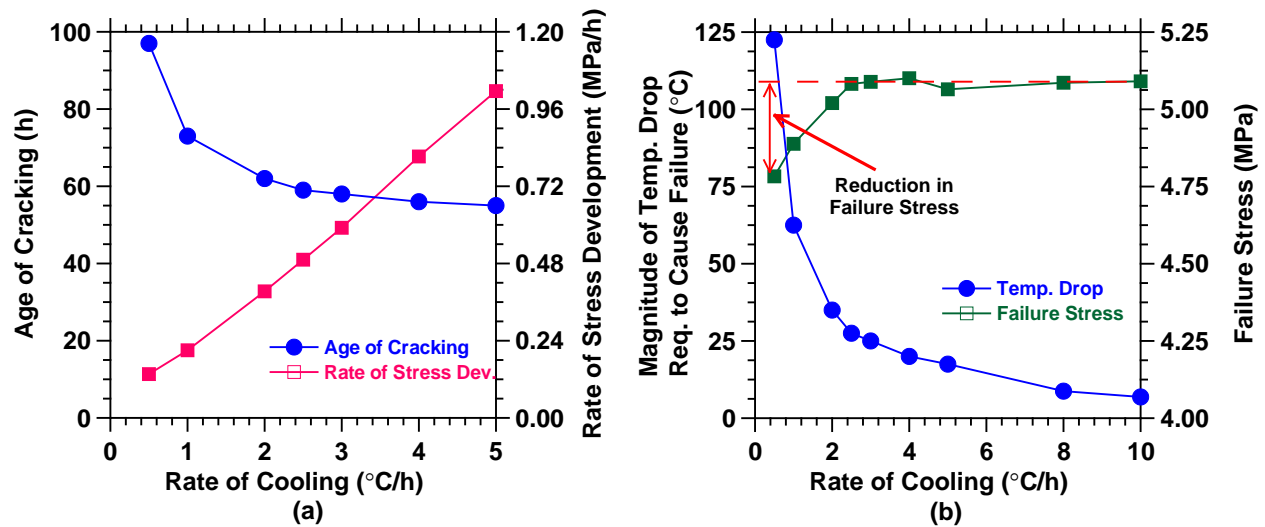
Fig. 12. Influence of the rate of cooling on (a) the stress development and the age of cracking, and (b) the magnitude of temperature reduction and the average stress at failure in the dual ring test.

4.4. Influence of creep and stress relaxation

Due to the lower stiffness of the LWA, the creep and stress relaxation of mortar materials containing LWA is generally expected to increase with increasing the volume of low-stiffness LWA [22, 41]. However, the increase in cement hydration due to the internal curing results in a reduction in the creep and stress relaxation of mortar materials [52]. As such, the net effect of pre-wetted LWA on the creep and stress relaxation of mortar materials depends on both the volume of low-stiffness LWA and the beneficial contribution of the internal curing on cement hydration. A series of simulations was performed to assess the influence of stress relaxation on the stress development and cracking potential in the dual ring test. The coefficients of the Maxwell Chain Model for the plain mortar were modified to increase the stress relaxation. The percent increase in stress relaxation relative to the plain mortar was then calculated by comparing the calculated relaxed stresses with the stress development of the plain mortar specimen. Five different cases with increasing stress relaxations of 5 %, 13 %, 22 %, 32 %, and 42 % were simulated as designated by R-5, R-13, R-22, R-32, and R-42 in Table 1, respectively. It should be noted that the only difference in each case was the level of stress relaxation.

Fig. 13a shows the influence of the stress relaxation on the rate of stress development in the dual ring specimens. As expected, when the stress relaxation increased, stresses developed at a lower rate, the magnitude of the temperature drop to induce cracking was increased (Fig. 13b), and cracking occurred at a later age, resulting in a lower cracking potential at higher levels of stress relaxation. Fig. 13b shows that the average stress of specimens at failure decreased linearly with increasing the stress relaxation. This can be attributed to an increase in the compliance of cracks with increasing the stress relaxation, resulting in a stress redistribution and a concurrent reduction in the average stresses in the ring at the time of unstable cracking.
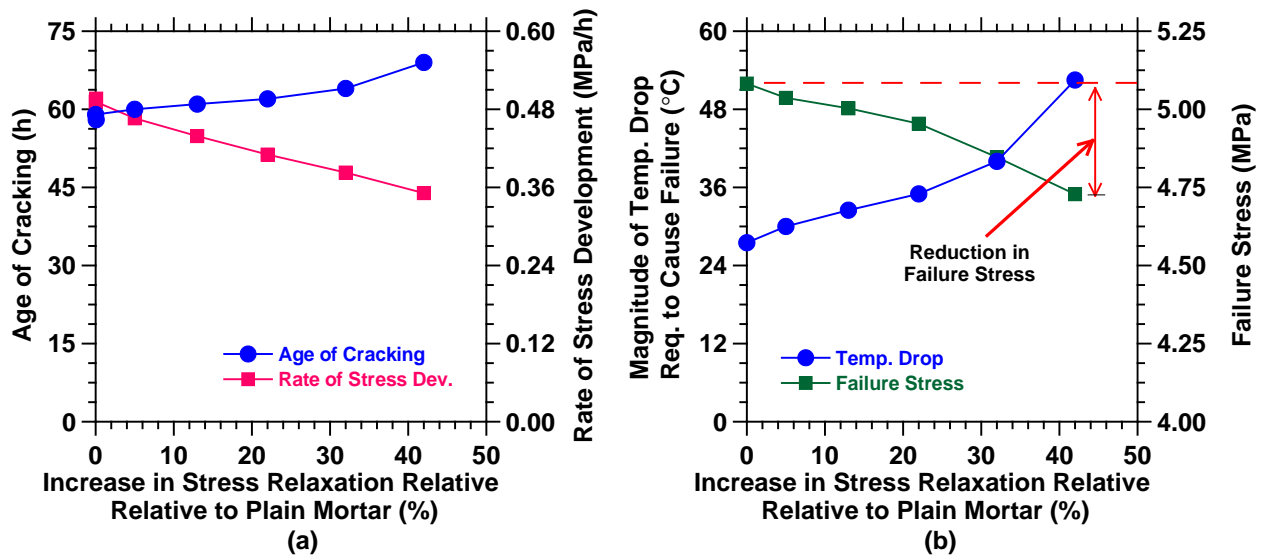
Fig. 13. Influence of stress relaxation on (a) the stress development and the age of cracking, and (b) the magnitude of temperature reduction and the average stress at failure in the dual ring test.

4.5. Influence of shrinkage of concrete

Thermal and shrinkage effects are known as two main causes of early-age cracking in concrete elements. When both thermal and shrinkage effects are present, both factors contribute to the stress development and cracking. The contribution of each factor to cracking can vary based on environmental conditions and mixture properties.

A series of simulations was performed to illustrate the influence of the magnitude of autogenous shrinkage on the thermal cracking behavior in the dual ring test. Seven different cases were simulated. The primary difference between the simulations was the magnitude of the autogenous shrinkage. The input shrinkage values for each case were modified by -140 %, -120 %, -60 %, -40 %, -20 %, +20 %, +40 %, and +60 % as designated by Sh+102, Sh+51, Sh-102, Sh-153, Sh-204, Sh-306, Sh-357, and Sh-408, respectively. The number following the "Sh" letters in these designations indicates the value of autogenous shrinkage at 48 h. All other model inputs were held the same as those of the plain mortar as indicated in Table 1. The cooling began after 48 h from the time of casting in all cases. As such, the specimens were only subjected to autogenous shrinkage deformations during the first 48 h, while they were subjected to simultaneous shrinkage and temperature deformations after 48 h. It should be noted that the Sh+102 and Sh+51 specimens simulate thermal stress development in specimens that were subjected to an initial autogenous expansion.

Fig. 14a illustrates the influence of shrinkage on the stress development and cracking in the dual ring test. The stress development in all specimens, as expected, was proportional to the autogenous shrinkage values during the first 48 h. For example, the stress level in Sh+102 specimen with a shrinkage level of +102 $\mu\varepsilon$ at 48 h was -0.22 MPa (the negative sign indicates compressive stress) while the stress level in the Sh-306 specimen with a 48 h shrinkage level of -306 $\mu\varepsilon$ was 3.96 MPa. It should be noted that due to their high shrinkage intensities, the Sh-357 and Sh-408 specimens cracked 38 h and 21 h after the time of casting, respectively. As such, they were not subjected to thermal loading.

Once the cooling started, stresses began to increase at the rate of 0.518 MPa/h in all specimens (Fig. 14a). However, the rate of stress development began to decrease once the shrinkage magnitude exceeded 204 $\mu\varepsilon$ at 48 h. For example, the rate of stress development is reduced to 0.456 MPa/h in the case of Sh-306 specimen. This can be explained by the formation of shrinkage induced cracks before the cooling began at 48 h. When shrinkage induced stresses reached the tensile strength at the inner surface of the Sh-306 specimen at 36 h, cracking began and propagated in a stable fashion in the specimen. The growth of the crack between 36 h and 48 h (when the cooling began) reduced the stiffness of the specimen, resulting in a slower rate of stress development once the cooling started. It should be noted that the specimens with higher

shrinkage intensities (i.e., the Sh-357 and Sh-408 specimens) cracked before cooling began and are not discussed further.

The influence of autogenous shrinkage on the average stresses at the failure of the dual ring specimens is illustrated in Fig. 14b. Due to the high rate of cooling (i.e., 2.5˚C/h), no significant stress redistribution occurred and the average section stress of the specimens remained insensitive to the autogenous shrinkage. Fig 14b shows that the magnitude of temperature drop decreased linearly with an increase in the autogenous shrinkage of the specimens. The specimens were more prone to thermal cracking when they were exposed to high levels of shrinkage-induced stresses before the start of cooling. In contrast and as expected, the specimens that experienced early-age autogenous expansion illustrated a better thermal cracking performance and cracked last (Fig. 14a).
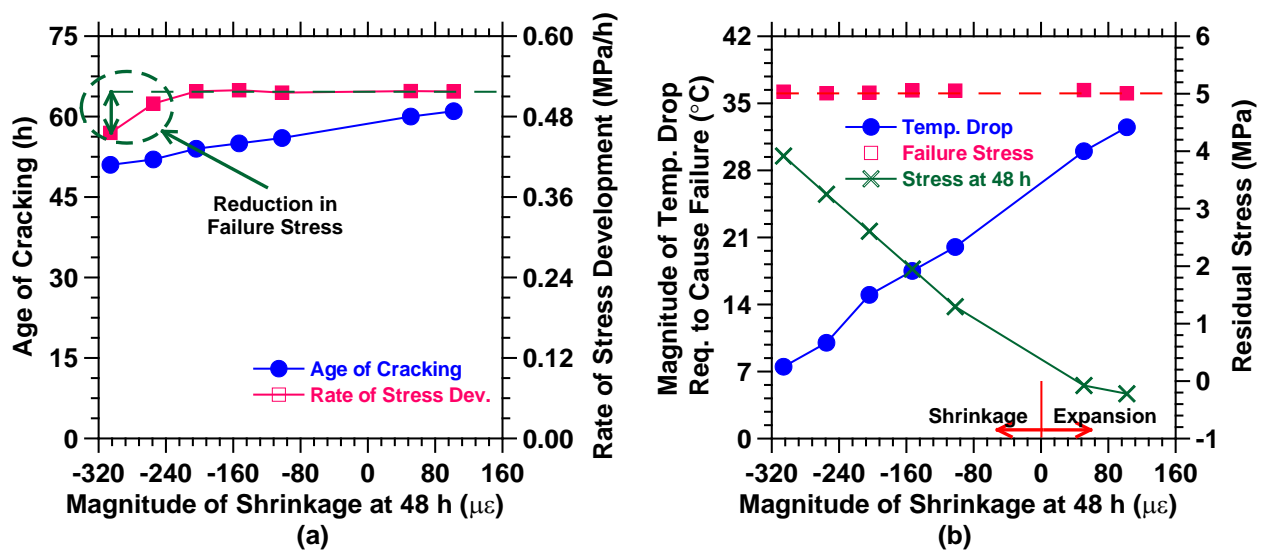
Fig. 14. Influence of autogenous shrinkage on (a) the stress development and the age of cracking, (b) the magnitude of temperature reduction, stresses at 48 h, and the average section stress at failure in dual ring test.

4.6. Influence of thermal heat capacity

It has been reported that the specific heat capacity of concrete is a function of the water content and density of concrete [6]. As a result, the heat capacity of concrete made with pre-

wetted LWA is expected to increase with the amount of internal curing water and reduce with increasing the volume of low-density LWA. In order to determine the influence of variations in the volumetric heat capacity on the rate of thermal stress development in the dual-ring test, another series of simulations was performed. As shown in Table 1, four cases were modeled in addition to the base case specimen, where the primary difference between each case was the value of heat capacity. The magnitude of the volumetric heat capacity of the plain mortar (i.e., base case specimen), 2100 kJ/(m^3·K), was varied by ±10 % and ±20 % in each simulation. The results indicated that the thermal stress development and cracking behavior of the specimen in the dual ring test were not sensitive to the changes in heat capacity. This can be explained by the fact that dual ring test is a temperature controlled test. Since it was the temperature of the system that was controlled (not the amount of heat flow from the system), the heat capacity of the specimen was not a significant material property in the dual ring testing.

5. Conclusions

The dual ring geometry was modeled using finite element analysis. A parametric study was performed to explain the thermal cracking behavior of concrete mixtures containing pre-wetted lightweight aggregates. The following conclusions can be made based on the simulation results.

Stresses developed at a slower rate and cracking occurred at a later age when the elastic modulus of concrete was reduced (i.e., the concrete was more compliant). As such, a larger temperature drop was needed to crack the specimen with a lower elastic modulus. Due to the higher compliance, significant unloading and stress redistribution was observed during crack propagation in the dual ring specimen with a reduced elastic modulus. This resulted in a lower average concrete section stress at the time of failure. This behavior became more significant when the elastic modulus of concrete was reduced by more than 20 % and greater stress relaxation occurred.

Stress development and cracking behavior were influenced by the COTE of the specimen and the COTE of the restraining rings. It was determined that the rate of stress development in the dual ring test was directly proportional to the difference between the COTEs of the specimen and that of the restraining rings. When the COTE of the restraining rings was increased, stresses

developed at a slower rate. As a result, the thermal cracking resistance of concrete can be viewed as being artificially improved by using a restraining ring with a high COTE value. Consequently, it is recommended that Invar or other materials with minimal COTE need to be used to minimize this testing effect.

As expected, the rate of stress development was proportional to the rate of cooling in the dual ring test. As the rate of cooling of the specimen was reduced, a higher temperature drop was needed to crack the specimen. It was shown that cracking may or may not occur in a dual ring specimen, depending on the rate of cooling. The slowest rate of cooling recommended is 2.5 °C/h. When the cooling rate exceeded 8 °C/h, a considerable temperature difference between the center and boundary of the specimen developed. To limit the thermal stress gradient through the concrete cross section, it is recommended to keep the cooling rate below 8.0 °C/h.

When the stress relaxation and creep of the specimen were increased, the rate of stress development was reduced and a higher temperature drop was needed to crack the specimen. Higher stress relaxation resulted in a more compliant crack and corresponding stress redistribution and unloading in the cracked region.

The thermal cracking performance of the specimens improved with reducing their autogenous shrinkage. While the magnitude of shrinkage did not affect the rate of stress development, the temperature drop necessary to induce cracking was increased when decreasing the autogenous shrinkage. At high shrinkage levels, the presence of shrinkage induced cracks reduced the stiffness of the specimen, thereby reducing the rate of thermal stress development when the cooling was initiated.

Acknowledgements

References

[1] ACI-207.2R-95. Effect of Restraint, Volume Change, and Reinforcement on Cracking of Mass Concrete. ACI2072R-95: American Concrete Inst.; 1995.

[2] Springenschmid R. Prevention of Thermal Cracking in Concrete at Early Ages (RILEM Report, 15) Spon Press; 1998. p. 368

[3] Moon JH, Rajabipour F, Pease B, Weiss J. Quantifying the Influence of Specimen Geometry on the Results of the Restrained Ring Test. Journal of ASTM International. 2006;3(8):1-14.

[4] Weiss WJ. Prediction of Early-age Shrinkage Cracking in Concrete. Evanston, Northwestern University; 1999.

[5] Raoufi K, Bernard ES, Weiss J. Shrinkage Cracking Behavior of Fiber Reinforced Concrete: As Assessed Using the Restrained Ring Test. Journal of ASTM International. 2010;7(7):15.

[6] Bentz DP. A review of early-age properties of cement-based materials. Cement and Concrete Research. 2008;38(2):196-204.

[7] Raoufi K. Saw-cutting guidelines for concrete pavements: examining the requirements for time and depth of saw-cutting. West Lafayette, Purdue University; 2007.

[8] Raoufi K, Weiss J, Nantung T. Numerical assessment of saw-cutting: The influence on stress development and cracking. Pavement Cracking: Mechanisms, Modeling, Detection, Testing and Case Histories. 2008:109-18.

[9] Schlitter J, Senter A, Bentz D, Nantung T, Weiss WJ. A Dual Concentric Ring Test for Evaluating Residual Stress Development Due to Restrained Volume Change. Journal of ASTM International. 2010a;7(9):13.

[10] Bentz DP, Sant G, Weiss J. Early-age properties of cement-based materials. I: Influence of cement fineness. Journal of Materials in Civil Engineering. 2008;20(7):502-8.

[11] Weiss J, Lura P, Rajabipour F, Sant G. Performance of shrinkage-reducing admixtures at different humidities and at early ages. ACI Materials Journal. 2008;105(5):478-86.

[12] Guillaume C. Invar and its applications - Preliminary. Nature. 1905;71:134-9.

[13] Lement BS, Averbach BL, Cohen M. The Dimensional Behavior of Invar. Transactions of the American Society for Metals. 1951;43:1072-97.

[14] Nakamura Y. Invar Problem. IEEE Transactions on Magnetics. 1976;12(4):278-91.

[15] Radlinska A, Bucher B, Weiss J. Comments on the interpretation of results from the restrained ring test. Journal of ASTM International. 2008;5(10):12.

[16] Pease B. The Role of Shrinkage Reducing Admixtures on Shrinkage, Stress Development, and Cracking. West Lafayette, Purdue University; 2005.

[17] Radlinska A, Moon J, Rajabipour F, Weiss J. The ring test: a review of recent developments. In: Jensen OM, Lura P, Kovler K, editors. International RILEM Conference on Volume Changes of Hardening Concrete: Testing and Mitigation2006. p. 9.

[18] Kim S, Sargand S, Wargo A. A simple test procedure for evaluating low temperature crack resistance of asphalt concrete. Columbus, OH: Ohio Department of Transportation; 2009.

[19] Schlitter J, Barrett T, Weiss W. Restrained shrinkage behavior due to combined autogenous and thermal effects in mortars containing super absorbent polymer (SAP). International RILEM Conference on Use of Superabsorbent Polymers and Other New Additives in Concrete. Technical University of Denmark, Lyngby, Denmark2010d.

[20] Bentz DP, Jensen OM. Mitigation strategies for autogenous shrinkage cracking. Cement & Concrete Composites. 2004;26(6):677-85.

[21] RILEM-TC-196. Internal curing of concrete, state-of-the-art report of RILEM technical committee 196-ICC. France, Bagneux RILEM Publications S.A.R.L.; 2007.

[22] Shin K, Bucher B, Weiss J. The Role of Lightweight Synthetic Particles on the Restrained Shrinkage Cracking Behavior of Mortar ASCE Journal of Materials in Civil Engineering. 2010;In Press.

[23] Schlitter J. New Methods to Quantify the Cracking Performance of Cementitious Systems Made with Internal Curing. West Lafayette, Purdue University; 2010c.

[24] Raoufi K. Restrained Shrinkage Cracking Of Concrete: The Influence of Damage Localization. West Lafayette, Purdue University; 2010.

[25] FEMMASSE-MLS8.5-User-Manual. Finite Element Modules for Material Science and Structural Engineering. Netherland: MLS Version 8.5, FEMMASSE B.V.; 2006.

[26] ASTM-C1581-09a. ASTM-C1581-09a: Standard Test Method for Determining Age at Cracking and Induced Tensile Stress Characteristics of Mortar and Concrete under Restrained Shrinkage. Annual Book of ASTM Standards. West Conshohocken, PA: ASTM International; 2009. p. 966.

[27] Schlitter J, Bentz D, Weiss WJ. Quantifying Reserve Cracking Capacity Using a Dual Ring Device and a Temperature Drop (IN PROGRESS). ACI Materials Journal. 2010b.

[28] Hossain AB, Weiss J. Assessing residual stress development and stress relaxation in restrained concrete ring specimens. Cement & Concrete Composites. 2004;26(5):531-40.

[29] ASTM-C496-04. Standard Test Methods for Splitting Tensile Strength of Cylindrical Concrete Specimens. Annual Book of ASTM Standards. West Conshohocken, PA: ASTM International; 2009. p. 966.

[30] ASTM-C469-02. Standard Test Method for Static Modulus of Elasticity and Poisson's Ratio of Concrete in Compression. Annual Book of ASTM Standards. West Conshohocken, PA: ASTM International; 2009. p. 966.

[31] ASTM-C1698-09. Standard Test Method for Autogenous Strain of Cement Paste and Mortar. Annual Book of ASTM Standards. West Conshohocken, PA: ASTM International; 2009. p. 966.

[32] ASTM-C403-08. Standard Test Method for Time of Setting of Concrete Mixtures by Penetration Resistance. Annual Book of ASTM Standards. West Conshohocken, PA: ASTM International; 2009. p. 966.

[33] SYSTAT. TableCurve 2D. Automated Curve Fitting & Equation Discovery. 5.01 ed: SYSTAT Software Inc.; 2002.

[34] ASTM-C490/C490M–09. Standard Practice for Use of Apparatus for the Determination of Length Change of Hardened Cement Paste, Mortar, and Concrete. West Conshohocken, PA: ASTM International; 2009. p. 966.

[35] ACI-Committee-213. ACI 213R-03: Guide for Structural Lightweight-Aggregate Concrete. ACI-213R-03: American Concrete Inst.; 2003.

[36] Martin I. Environment Effect on Thermal Variations and Shrinkage of Lightweight Concrete Structures. ACI Journal Proceedings. 1972;69(3):179-84.

[37] Riding KA, Poole JL, Schindler AK, Juenger MCG, Folliard KJ. Effects of Construction Time and Coarse Aggregate on Bridge Deck Cracking. ACI Materials of Journal. 2009;106(5):448-54.

[38] Van Breugel K. Prediction of Temperature Development in Hardening Concrete. In: Springenschmid R, editor. Prevention of Thermal Cracking in Concrete at Early Ages. London: E & FN Spon; 1998. p. 51-75.

[39] Østergaard L. Early-Age Fracture Mechanics And Cracking of Concrete Experiments and Modeling, Technical University of Denmark; 2003.

[40] Findley W, Lai J, Onaran K. Creep and Relaxation of Nonlinear Viscoelastic Materials: with an Introduction to Linear Viscoelasticity. NY: Dover Publications; 1989.

[41] Hobbs D. The dependence of the bulk modulus, Young's modulus, creep, shrinkage and thermal expansion of concrete upon aggregate volume concentration. Materials and Structures. 1971;4(20):107-14.

[42] Henkensiefken R. Internal curing in cementitious systems made using saturated lightweight aggregate. West Lafayette, Purdue University; 2008.

[43] Moon JH, Weiss J. Estimating residual stress in the restrained ring test under circumferential drying. Cement & Concrete Composites. 2006;28(5):486-96.

[44] Neville A. Properties of Concrete: Fourth and Final Edition. fourth ed: Wiley; 1996.

[45] Khan A, Cook W, Mitchell D. Thermal Properties and Transient Thermal Analysis of Structural Members During Hydration. ACI Materials Journal. 1998;95(3):293-303.

[46] Shah S, Swartz S, Ouyang C. Fracture Mechanics of Concrete: Applications of Fracture Mechanics to Concrete, Rock and Other Quasi-Brittle Materials: John Wiley & Sons Inc.; 1995.

[47] Attiogbe E, Weiss J, See H. A look at the rate of stress versus time of cracking relationship observed in the restrained ring test. Proceedings of the international RILEM symposium on advances in concrete through science and engineering. Evanston, Illinois2004.

[48] Jenq YH, Shah SP. Two-Parameter Fracture Model for Concrete. ASCE Journal of Engineering Mechanics. 1985;111(10):1227-41.

[49] Wittmann F, Roelfstra P, Mihashi H, Huang Y, Zhang X, Nomura N. Influence of age of loading, water-cement ratio and rate of loading on fracture energy of concrete Materials and Structures. 1987;20(2):103-10.

[50] Bazant ZP, Gettu R. Rate Effects and Load Relaxation in Static Fracture of Concrete. ACI Materials Journal. 1992;89(5):456-68.

[51] Emborg M. Development of Mechanical Behaviour at Early Ages. In: Springenschmid R, editor. Prevention of Thermal Cracking in Concrete at Early Ages (RILEM Report, 15) London: Spon Press; 1998. p. 76-148

[52] Lopez M, Kahn LF, Kurtis KE. Effect of internally stored water on creep of high-performance concrete. ACI Materials Journal. 2008;105(3):265-73.